Tangential electrostatic field at metal surfaces

Yuanjie Huang*

Mianyang, *Sichun province*, *People's Republic of China*

*Corresponding author's E-mail: hyj201207@163.com

As is well-known for more than a hundred years, when electrostatic equilibrium is reached, the electrostatic field outside a metal is always perpendicular to the metal surface and there is no component parallel to the metal surface. However, unexpectedly, in this work the electrostatic field parallel to metal surface, *i.e*., the tangential electrostatic field (TEF) at metal surface, may be discovered by means of mechanical-electric coupling which may originate from the strain dependent of Fermi surface energy (FSE) in metals. Further investigations indicates that the TEF at metal surface may give birth to interesting physical effects such as TEF causing variations for photoelectron emission spectroscopy, TEF-induced redistribution of minority atoms, TEF-induced Reshba effect and so on. Moreover, an electron double-dipole resonance (EDDR) mechanism may be uncovered based on the electrostatic field at the surfaces of metal nanoparticles. To one's surprise, using EDDR a simple unified model might be constructed for the longstanding problem in physics and chemistry, *i.e*, surface-enhanced Raman scattering (SERS). And this unified model could provide satisfactory explanations for the main experimental phenomena on SERS. In a word, the newly unraveled TEF at metal surface in this work may enable people to re-understand the metal surface in electrostatic field and explore subsequent important mechanical, physical and chemical effects in various areas.

keywords: tangential electrostatic field, metal surface, mechanical-electric coupling, Fermi surface energy, surface-enhanced Raman scattering, electron double-dipole resonance

1. Introduction

In the area of electromagnetism, it was long believed that when electrostatic equilibrium is reached, the electrostatic field inside a metal is rigorously zero, leading to the results that a metal is an equipotential body and there is no net electric charges inside the metal [1, 2, 3, 4]. The electrostatic equilibrium for a metal requires that the electrical current in the metal is zero, so that the electric field in the meal must be zero according to the famous Ohm's law [1, 2, 3, 4]. Otherwise, any remnant electric field would urge free electrons to move, forming an electrical current in the metal [1, 2, 3, 4], which violates against the electrostatic equilibrium.

The question is "Does any internal electric field inevitably cause an electrical current in a metal?". By means of investigation, it was found that the internal electric field does not always cause an electrical current in a metal and sometimes the electrical current is zero even if there exists strong electrostatic field in the metal. This point was revealed and gave birth to a new discovery of a mechanical-electric coupling in metals, *i.e.*, *Yuheng Zhang effect* [5]. This effect first pointed out that any actual metal may no longer be an equipotential body and there always exists an electric field inside the metal even at electrostatic equilibrium in view of widespread dislocations and other type of strains [5, 6, 7]. At electrostatic equilibrium, the electrostatic field inside the metals may be given by *Yuheng Zhang equation* [5, 6],

$$\nabla E_F = e\vec{E} \tag{1}$$

where E_F is Fermi surface energy (FSE), namely, electron chemical potential and sometimes it is known as Fermi level, e is electron charge, $\vec{E}$ is the electrostatic field.

The existence of the electrostatic field inside metals may bring interesting physical effects which were discussed [5, 6].

On the other hand, for the situations of electrostatic field at actual metal surfaces, the classical electrostatic theory showed that the electrostatic field must be always perpendicular to the metal surfaces and there is no tangential component along metal surfaces [1, 2, 3, 4]. If there were a tangential component, no matter how weak it is, the free electrons would move along the metal surface and an electrical current would emerge [1, 2, 3, 4], as is forbidden by the electrostatic equilibrium.

However, enlightened by *Yuheng Zhang effect* [5], electrostatic equilibrium only requires the zero electrical current in metals but may permit existence of electrostatic field. Likewise, at the metal surfaces, electrostatic equilibrium forbids any electrical current along metal surfaces but may also allow the tangential component, meaning that sometimes the tangential component does not generate an electrical current.

In this work, the presence of the tangential electrostatic field (TEF) along metal surfaces will be uncovered and the subsequent physical effects will be studied in various fields.

2. Results and Discussion

Even at single-crystalline metal surfaces, there still exists many factors such as residual stresses [8, 9], defects [10], composition difference, different temperatures, chemical adsorption and so on which may alter the FSE E_F, *i.e.*, electron chemical potential. As a result, the free electrons in the metal may move from the higher-FSE regions to lower-FSE regions. The transfer of electrons would produce an electrical

current and also cause an electric field between the higher-FSE regions and lower-FSE regions based on Gauss' law. The generated electrical current may be written as

$$\vec{J} = \sigma(0)\vec{E} - \frac{\sigma(0)}{e}\nabla E_F \tag{2}$$

where J is electrical current density, $\sigma(0)$ is direct-current electric conductivity of the metal. In this equation, the first term on the right denotes the electrical current generated by electric field, whereas the second term originate from the directional electron transfer induced by alteration of FSE. When electrostatic equilibrium is approached, the electric current must be zero, thereby resulting in an electrostatic field in the metal. Of emphasized is that for low-dimensional materials the electron transfer usually affect FSE, so the position dependence of FSE in Equations (1) and (2) may take the values at electrostatic equilibrium, which has taken electron transfer effect on FSE into account.

By means of Equations (1) and (2), one may find that the absence of electrical current in a metal at electrostatic equilibrium could allow the presence of an electrostatic field. Similarly, in the case of metal surface at electrostatic equilibrium, Equations (1) and (2) also reveal that the zero electrical current at metal surface permits a TEF which may arise from related alterations of FSE. Therefore, the electrostatic field may not be always normal to metal surfaces, but a TEF resulting from lift of FSE may appear along metal surfaces, as is illustrated in Figure 1. The existence of TEF may agree with the carefully performed experiments which revealed the existence of surface potential variations in the order of a few millivolts at metal

surfaces (Sometimes the surface potential variations at metal surfaces is referred to Patch effect.) [11, 12, 13].

The existence of TEF along metal surfaces may give birth to interesting physical effects, as will be discussed in the followings.

2.1 Electric transport properties at surfaces

When an external voltage is applied to the metal surface shown in Figure 1 and form an electrical circuit shown in Figure 2. In analogy with the situation for interior of metal with different FSE, the electrical current-voltage (*I*-*V*) relation of the metal surface may exhibit rectifying characters. If a forward bias external voltage is applied as shown in Figure 2(a), the energy of free electrons in region III may be uplifted relative to that of free electrons in regions I, so that free electrons would drift from region III to regions I, creating an electrical current which is displayed in Figure 2(c). However, upon application of a small backward bias voltage, as shown in Figure 2(b), owing to that the free electron movement may be blocked by the energy barrier originating from the FSE difference, the electrical current may be almost zero except a tiny tunneling current. If the backward bias voltage increases to a critical value V_Z, the free electrons in region I may gain enough energy to surpass the energy barrier and reach region III easily, thereby forming a notable electrical current, as shown in Figure 2(c). And the critical voltage V_Z could be obtained by means of Equation (1)

$$V_Z = -\frac{1}{e}\left[E_F\left(\vec{r}_{III}\right) - E_F\left(\vec{r}_I\right)\right] \tag{3}$$

where e is electron charge, $E_F\left(\vec{r}_{III}\right), E_F\left(\vec{r}_I\right)$ are the FSE of region III and region I, respectively. It means that in presence of TEF the metal surfaces sometimes could

rectify electrical current and behave as a p-n junction. And the rectifying characters may be more obvious at low temperatures because of the suppression of thermal excitation.

For actual metal surfaces, complex strains, adsorptions, defects and so on may induce very complex TEF. As revealed, the fields could cause the rectifying characters and usually reduce the surface electrical conductivity, which may enlighten people that to obtain a relatively precise electrical conductivity of metal surface one had better employ a large electrical voltage and measure in both ways of forward bias and backward bias.

2.2 Rashba effect at metal surfaces

The Reshba effect first discovered in 1959 [14] describes a momentum-dependent spin splitting of electron states in a bulk crystal [14] and low dimensional electron systems [15]. For an electron system with space inversion-symmetry breaking, it is commonly described by the following Hamiltonian,

$$H_R = \alpha_R \vec{n} \cdot \left(\hat{\sigma} \times \vec{k} \right) \tag{4}$$

where $\vec{k}$ is the electron momentum, $\hat{\sigma}$ Pauli matrices, and $\vec{n}$ is unit vector along the surface normal, the parameter α_R is Rashba coupling which is usually proportional to the magnitude of electric field.

Based on the physics of Reshba effect, the TEF at metal surface may also contribute to the momentum-dependent spin slitting of electron bands, and the correlated Hamiltonian may be given by

$$H_{RZ} = \eta \nabla E_F \cdot \left(\hat{\sigma} \times \vec{k} \right) \tag{5}$$

where η is the coupling parameter with the unit m^2. Appearance of this Hamiltonian may further reduce the symmetry of electron spin bands in the momentum space. To examine its effect, the summation of Hamiltonian is

$$H_R = \frac{p^2}{2m_e} + \alpha_R \vec{n} \cdot \left(\hat{\sigma} \times \vec{k} \right) + \eta \nabla E_F \cdot \left(\hat{\sigma} \times \vec{k} \right) \tag{6}$$

Where p signifies the momentum operator. In terms of simple calculation, the eigenenergy is

$$E_{\pm}\left(\vec{k}\right) = \frac{\hbar^2 k^2}{2m_e} \pm \left| \left(\alpha_R \vec{n} + \eta \nabla E_F \right) \times \vec{k} \right| \tag{7}$$

It shows that in presence of TEF the momentum-dependent splitting of electron band may be shifted. When the tangential field vanished, the related eigenenergy would reduce to the familiar solutions for Rashba Hamiltonian, as inversely verifies the correctness of the above electron bands shown by Equation (7).

Due to the TEF in Equation (5), a spin component along the surface normal will emerge as

$$\left\langle \varphi_1 \left| S_Z \right| \varphi_1 \right\rangle = \frac{\hbar}{2} \frac{\eta \left(\vec{k} \times \nabla E_F \right) \cdot \vec{n}}{\left| \left(\alpha_R \vec{n} + \eta \nabla E_F \right) \times \vec{k} \right|} \tag{8}$$

where $|\varphi_1\rangle$, $\langle\varphi_1|$ is the eigenket and eigenbra, respectively, S_z the spin component normal to the surface.

Generally speaking, the magnitude of tangential field in many metals may not be so strong that its effect might be weaker than Rashba effect. But for some special situations where the Rashba Hamiltonian vanishes, *i.e.*, the zero Rashba coupling α_R, the eigenenergy for the 2D electron systems would be

$$E_{\pm}\left(\vec{k}\right)=\frac{\hbar^2k^2}{2m_e}\pm\left|\eta\nabla E_F\times\vec{k}\right| \tag{9}$$

The effective magnetic field is

$$\vec{B}_{eff}=\frac{2\eta}{g\mu_B}\left(\nabla E_F\times\vec{k}\right) \tag{10}$$

where g is the spin-g factor and has a value of about 2, μ_B the Bohr magneton. And the related electron spin component along surface normal is

$$\left\langle\varphi_1'\right|S_Z\left|\varphi_1'\right\rangle=\frac{\hbar}{2}\frac{\eta\left(\vec{k}\times\nabla E_F\right)\cdot\vec{n}}{\left|\eta\nabla E_F\times\vec{k}\right|} \tag{11}$$

where $|\varphi'_1\rangle$, $\langle\varphi'_1|$ is the corresponding eigenket and eigenbra. If the electrons only possess the momentum parallel to the surface and the normal component is zero. Very interestingly, for such a 2D electron system without magnetic field and vertical electric field, it indicates that presence of any TEF would give birth to a totally spin-polarized state along the surface normal and the electron spin polarization strongly depends on its momentum. At ground state, the electron spins are polarized and parallel to the effective magnetic field B_{eff} as shown in Figure 5. The effective magnetic field and related spin splitting energy might be detected by means of electron spin resonance (ESR) experiments which was successfully carried out to measure the spin splitting energy for a 2D electron systems [16]. For such a 2D electron system as displayed in Figure 5(a), the up spins would accumulate on the left side while the down spins would get together on the right side of the metal surface. On application of an external electrical voltage at metal surface, only the electrons with up spin are allowed to flow but the electrons with down spin are inhibited as illustrated by Figure 5(b). Hence, the metal surface with the TEF might be a platform

for anomalous quantum Hall effect.

2.3 Effect on the photoemission spectroscopy

According to electrostatics [1, 4], *i.e.*, circumstances in which no physical variables depend on time, one may have

$$\nabla \times \vec{E} = 0 \tag{4}$$

So the TEF along the metal surface may cause a related tangential component outside the surface as illustrated by black arrows in Figure 1. It may has an important effect on photoemission spectroscopy (PES).

Based on the physical theory of PES [17], a tangential field may affect PES in two ways. One is that it may change the detected kinetic energy of photoelectrons by the amount

$$\Delta E_{kin} = eV_0 \tag{5}$$

where ΔE_{kin} is the variation of kinetic energy of photoelectron, e is electron charge, V_0 is the potential difference between the positions of photoelectron emission point and electron analyzer. As is shown in Figure 3, because of the complexity for both the experimental design and the unknown distribution of TEF in real experimental metal surface, the precise value of kinetic energy variation may be difficult to get. But one may estimate its value to be

$$\left|\Delta E_{kin}\right| \le \left|E_F\left(\vec{r}_{III}\right) - E_F\left(\vec{r}_I\right)\right| \tag{6}$$

The other is that for the photoelectrons emitted out of surface the tangential field may result in alterations in their wave-vector component parallel to surface. It is

$$k_{\parallel}^{f} = \sqrt{\left(k_{\parallel}^{i}\right)^2 + 2m_e eV_{\parallel}/\hbar^2} \tag{7}$$

where m_e is electron mass, $\hbar$ is the reduced Plank constant, $k_{\parallel}^{i}, k_{\parallel}^{f}$ respectively denote wave-vector component parallel to the surface for the initial state and final state of a photoelectron, $V_{\parallel}$ is potential difference induced by the TEF component outside the surface between photoelectron emission point and electron analyzer and it is $V_{\parallel} = -\int_{r_f}^{r_i} \vec{E}_{\parallel}(\vec{r}) \cdot d\vec{r}$, where $\vec{E}_{\parallel}(\vec{r})$ is position dependence of TEF outside metal surface, r_f, r_i present positions of electron analyzer and photoelectron emission site, respectively. As indicated by Equation (7), the tangential field can indeed change the wave-vector component parallel to the surface. Despite lack of knowledge on the detailed electrostatic field near the metal surface, an estimation could be made and the alteration may be in the range

$$\left| \left(k_{\parallel}^{f}\right)^2 - \left(k_{\parallel}^{i}\right)^2 \right| \le \frac{2m_e}{\hbar^2} \left| E_F(\vec{r}_{III}) - E_F(\vec{r}_I) \right| \tag{8}$$

In view of Equations (6) and (8), one may find that a larger FSE difference and thus a stronger TEF at metal surface usually have a more notable effect on the PES. Even for the single-crystalline surface at a uniform temperature, there still exists the unavoidable strains arising from residual stresses and defects. For instance, the residual stresses are often reported to reach ~10^2 *MPa* [8, 9, 18, 19], which can yield a few thousandths of a strain [20]. For most metals, the mechanical-electric coupling strength $|\partial E_F/\partial \xi_{ii}|$ (ξ_{ii} is the main strain) may be in the range 1-10 *eV*, so the residual strains at metal surfaces could cause tens of millielectron volts for the potential difference. Magnitude of the potential difference at surface may place a noticeable restriction on the measurement precision of PES, which deserves attention in the

related experiments, *e.g.*, angle-resolved photoemission spectroscopy (ARPES).

Existence of the TEF at metal surface may hybridize the electron orbital wave functions, for instance, hybridization of *s*, *p* orbitals. According to perturbation theory, the hybridized *s*, *p* wave functions are (to first-order precision)

$$\psi_{ns}' \approx \psi_{ns} + \sum \frac{\left\langle \psi_{np} \left| e\vec{E} \cdot \vec{r} \right| \psi_{ns} \right\rangle}{E_{ns} - E_{np}} \psi_{np} \tag{9}$$

$$\psi_{np}' \approx \psi_{np} + \frac{\left\langle \psi_{ns} \left| e\vec{E} \cdot \vec{r} \right| \psi_{np} \right\rangle}{E_{np} - E_{ns}} \psi_{ns} \tag{10}$$

where Ψ_{ns}, Ψ_{np} are electron wave functions with main quantum number *n* and angular momentum *s*, *p*, and Ψ'_{ns}, Ψ'_{np} stand for corresponding hybridized wave functions.

This hybridization may affect the photoemission spectroscopy of metal surface. If the TEF is along *x* axis, the hybridization only exists between *s* and p_x electron orbitals. So the corrected p_x wave function has a component of *s* orbital wave function as shown in Equation (10). For a tetragonal metal surface with conductive *p* electrons, a beam of photons can be utilized to radiate the metal surface at a very small glancing angle (e.g. less than 5°) as shown in Figure 6. According to the ARPES theory [21], the measured ARPES intensity may be proportional to the square $\left|\left\langle \psi_f \left| \vec{A} \cdot \vec{P} \right| \psi_{np} \right\rangle\right|^2$, *i.e.*, $I \propto \left|\left\langle \psi_f \left| \vec{A} \cdot \vec{P} \right| \psi_{np} \right\rangle\right|^2$ where *A* is the electromagnetic gauge and *P* is the electron momentum. Considering the photon radiation at metal surface with tetragonal symmetry, symmetry analysis could be used to clarify contributions to APRES intensity. If the glancing photons have *s* polarization (photon electric field perpendicular to the scattering plane k_x-k_z)，the ARPES intensity contributed by the scattering matrix element is zero along k_y direction $\left|\left\langle \psi_f \left| \vec{A} \cdot \vec{P} \right| \psi_{np_x} \right\rangle\right|^2 = 0$, because

both the final state of photoelectron wave function Ψ_f and the term $\vec{A}\cdot\vec{P}$ lying in the mirror plane k_y-k_z is even, but Ψ_{npx} is odd relative to the mirror plane k_y-k_z. However, the presence of TEF along x axis may generate the hybridization between s electron orbital and p_x electron orbital as indicated by Equation (10), which enables the term $\left|\left\langle \psi_f \left| \vec{A}\cdot\vec{P} \right| \psi'_{np_x} \right\rangle\right|^2 > 0$ to contribute to ARPES intensity along k_y axis. In the related experiments, one may find that when the incident photons having s polarization are scattered in the k_x-k_z plane, the corresponding ARPES intensity along k_y axis may be more or less stronger than that along k_x axis.

2.4 Effect on the Scanning tunneling microscope or spectroscopy

The altered FSE and the correlated TEF may have a non-negligible influence on the scanning tunneling microscope or spectroscopy (STM/STS). And the tunneling current may be changed by the induced variations in density of state (DOS) and work function. For a region with altered FSE at a metal surface, a tunneling current may appear upon application of an electrical bias voltage V_{bias} on the sample at low temperatures, and it may be [22, 23]

$$I \approx \frac{4\pi e}{\hbar}\left|M\right|^2 N_t\left(\mu_0\right)\int d\varepsilon N_s\left(\varepsilon\right)\left[f\left(\varepsilon - eV_Z\right) - f\left(\varepsilon + eV_{bias} - eV_Z\right)\right] \qquad (11)$$

where M is the tunneling matrix element, $N_t(E_{F0})$ and $N_s(\varepsilon)$ are the density of states (DOS) of the tip at the FSE E_{F0} and the energy ε dependence of local density of states (LDOS) of the sample surface confronting the tip, respectively. f is Fermi-Dirac distribution function. The LDOS of the sample may be a slowly varying function, so Equation (11) could be simplified to be

$$I \approx \frac{4\pi e^2 V_{bias}}{\hbar}\left|M\right|^2 N_t\left(E_{F0}\right) N_S\left(E_F + eV_Z\right) \qquad (12)$$

where E_F is the altered FSE of the region, V_z is the electric potential between this region and surrounding regions with initial FSE E_{F0} as shown in Figure 4, and it is $E_F + eV_z = E_{F0}$. Based on Equation (12), one may find that for the region with altered FSE the tunneling current may be determined by its LDOS at the corresponding energy level ($E_F + eV_z$) instead of its LDOS at the FSE E_F.

On the other hand, owing to alteration in FSE, the work function of the electron at this region may be changed

$$\phi_s = \phi_{s0} + eV_Z \tag{13}$$

where ϕ_{s0}, ϕ_s denote the work function of metal surface with unaltered FSE and altered FSE, respectively. The variations of work function may further lift the tunneling current by changing the key parameter for the tunneling current, *i.e.*, inverse decay length, because the tunneling current is $I \propto e^{-2\kappa d}$ where κ is inverse decay length and d is distance between tip and sample surface [24]. The modified inverse decay length may be given [25, 26]

$$\kappa = \sqrt{\frac{2m_e}{\hbar^2}\left(\frac{\phi_t + \phi_{s0} + eV_Z}{2} - W + \frac{e|V_{bias}|}{2}\right)} \tag{14}$$

where W is the energy of the state relative to the FSE E_F. As is shown in this equation, regions of metal surface with up-shift FSE would be expected to yield a rising tunneling current and vice versa. These regions may be detected by the constant height mode of operation for STM.

2.5 Surface transport and segregation

Analogous to the case in metals [27], the TEF at surface of metallic terminal solid solution (MTSS) may also cause a composition segregation. For simplicity, the MTSS

could be selected to be composed of only two different types of atoms. For the minority atoms at MTSS surface, their diffusion flux could be given by the famous Fick's law [28]

$$j_0 = -D\nabla n\left(\vec{r},t\right) \tag{15}$$

where $n(r, t)$ is position r and time t dependence of minority atom concentration, D is diffusion constant at surface. Based on Einstein diffusion relation, the diffusion constant equal to $D=uk_BT$, where k_B is Boltzmann constant, T is temperature, and u is the mobility of minority atom at alloy surface.

In view of possible TEF at surfaces, the field-induced another transport mechanism may play an important role in the evolution processes of surface composition. In the following discussions, only considered is the electric field originating from inhomogeneous strain and composition distribution in terms of *Yuheng Zhang equation*, although there may usually exist many such factors that enable the FSE to shift and thereby induce a related electric field. By employing Equation (1), the electric field generated by the non-uniform strain at a surface normal to z axis may be

$$\vec{E}_1 = \frac{1}{e}\frac{dE_F}{d\xi_{zi}}\nabla\xi_{zi} \tag{16}$$

where ξ_{zi} ($i=x, y, z$) is the strain components at the surface normal to z axis and the subscript indices obey Einstein summation rules, $dE_F/d\xi_{zi}$ denotes the mechanical-electric coupling of the MTSS. According to T. Teorell's theory [29], the electric field would result in a correlated drift term and it is

$$j_1 = n(\vec{r},t)u\frac{Q}{e}\frac{dE_F}{d\xi_{zi}}\nabla\xi_{zi} \tag{17}$$

where Q denotes the charges carried by a minority atom due to the electronegativity differences between the minority atoms and majority atoms.

In terms of Equation (1), the inhomogeneous distribution of minority atoms at the MTSS surface may also give rise to a tangential electric field along the surface and it may be

$$\vec{E}_2 = \frac{1}{e}\frac{dE_F}{dn}\nabla n(\vec{r},t) \tag{18}$$

where e is electron charge, E_F is minority atom concentration dependence of FSE. Likewise, this field may create another drift flux of the minority atoms and it may be given by

$$j_2 = n(\vec{r},t)u\frac{Q}{e}\frac{dE_F}{dn}\nabla n(\vec{r},t) \tag{19}$$

The total transport flux of the minority atoms at the TMSS surface may be the summation of diffusion term and the two drift terms,

$$j_t = -D\left[1-\alpha n(\vec{r},t)\right]\nabla n(\vec{r},t) + n(\vec{r},t)\frac{D}{k_BT}\frac{Q}{e}\frac{dE_F}{d\xi_{zi}}\nabla\xi_{zi} \tag{20}$$

where the parameter is $\alpha=Q(dE_F/dn)/ek_BT$. When the equilibrium state is approached, the total transport flux of the atoms at the MTSS surface may be rigorously zero. So, the distribution of minority atoms at MTSS surface could be obtained analytically

$$n(\vec{r}) = -\frac{1}{\alpha}ProductLog\left[-\alpha n(\vec{r}_0)exp\left(\frac{Q\Delta E_F}{ek_BT} - \alpha n(\vec{r}_0)\right)\right] \tag{21}$$

where the mathematical function is defined as $ProductLog(\lambda e^{\lambda})=\lambda$, the FSE difference ΔE_F stemming from strains is $\Delta E_F=E_F(r)-E_F(r_0)$. It can be seen that the existence of a

TEF at MTSS surface may induce a segregation of surface composition, which may further influence the physical properties and chemical properties of the surface. If the magnitude of the product is always very small $|\alpha n(r)| \ll 1$, this equation could be simplified to be

$$n\left(\vec{r}\right) \approx n\left(r_0\right) e^{Q\Delta E_F / ek_B T} \tag{22}$$

It may indicate that the composition distribution at MTSS surface may be controlled by temperature *T*, electronegativity difference and the shifted FSE caused by strain regardless of its physical sources. At high temperatures, the composition distribution at surface may be much more uniform than that at low temperatures. A smaller electronegativity difference between minority atoms and majority atoms may lead to a relatively uniform composition distribution and vice versa. In general, the continuous solid solutions [30] listed in Table 1 may exhibit a much more uniform composition distribution, whereas discontinuous solid solutions especially those with small solid solubility usually display serious composition segregation. This may be consistent with investigations on the surface segregation of bimetallic nanoparticles [31]. Another important factor is FSE difference sometimes induced by strains which is popular and usually encountered at MTSS surface because of residual stresses and various types of defects such as dislocations. Here a preliminary estimation may be helpful and necessary. Usually the residual stresses could reach several hundred MPa [8, 9, 18, 19], so the residual strain may be several thousandths. For most MTSS, the mechanical-electric coupling strength may be in the range 1-10 *eV*, thereby creating a FSE difference ΔE_F in the range 5 *meV*~50 *meV* at surfaces, as agrees with the

experimentally observed magnitude of surface potential variations [11, 12, 13]. If the net charge carried by a minority atom is an electron charge, the room-temperature-composition segregation ratio at surface might reach 1.2~7 according to Equation (22), which may be in qualitative accordance with the segregation ratio induced by the enrichment of Pt atoms at edges and corners at nanoparticle surfaces [32, 33]. In the other respect, the more commonly observed is the radial strain reaching ~1% for many nanoparticles, so a FSE difference ΔE_F 10 *meV*~100 *meV* may be yielded along radius of nanoparticles. If the net charge carried by a minority atom is also an electron charge, the room-temperature segregation ratio estimated by Equation (22) may be in the range 1.5~50, which is consistent with experimental investigations on segregation ratio in bimetallic nanoparticles [31, 34]. The above estimations may prove rationality of Equation (22) in spite of their roughness. To get much more precise segregation ratio by using Equation (22), one should obtain more accurate parameters Q and ΔE_F.

2.6 Effect on field emission

Field emission is an important technique and has been applied in numerous areas such as field emission microscopy. Under externally applied strong electric field as shown in Figure 7(a), the electrons in a cold metal can tunnel into vacuum and form an electrical current. According to the famous field emission model proposed by Fowler-Nordheim [35], the current is

$$I = \frac{4\sqrt{\varepsilon_F \phi}}{(\varepsilon_F + \phi)} \frac{e^3 E}{16\pi^2 \hbar \phi} \exp\left(-\frac{4\sqrt{2m_e}\phi^{3/2}}{3\hbar e E} \right) \tag{23}$$

where ε_F is Fermi energy, *i.e.*, the largest kinetic energy for free electrons in a metal at

zero temperature, ϕ the work function, E the applied intense electric field at metal surface, e presents the electron charge.

Field emission process of a cold metal may be affected by existence of TEF at metal surface from two respects. As displayed by Figure7 (b), one is the shifted FES whose variations may correspond to changes of work function at low temperature. The other is the weak modifications on applied intense electric field at metal surface. The updated electrical current due to field emission may be given by

$$I' = \frac{4\sqrt{\varepsilon'_F\left(\phi-\Delta E_F\right)}}{\left[\varepsilon'_F+\left(\phi-\Delta E_F\right)\right]}\frac{e^3\left(E-E_0\right)}{16\pi^2\hbar\phi}\exp\left(-\frac{4\sqrt{2m_e}\left(\phi-\Delta E_F\right)^{3/2}}{3\hbar e\left(E-E_0\right)}\right) \tag{24}$$

where ε'_F is the shifted Fermi energy, ΔE_F is the lifted amount of FSE, E_0 denotes the electric field arising from the shifted FSE and it may be much weaker than the applied intense field. As is shown in this equation, the up-lifted FSE region at metal surface may generate a larger field emission current, because the related work function may be weakened, but the down-lifted FSE region may cause a smaller field emission current. For material surfaces such as nanoparticle surfaces, experiments and simulations indicated that a smaller radius of curvature usually yield a larger local strain [36, 37, 38, 39, 40, 41, 42]. According to the mechanical-electric coupling in metals, i.e., *Yuheng Zhang effect*, the noticeable local strain may lead to an apparent shift of FSE. Therefore, it could be inferred that both the intense field and up-shifted FSE due to notable local strain play an important role in the field emission of a sharp tip with a radius of curvature in nanoscale.

2.7 Micro-earth

Experimental and theoretical investigations indicated that a dramatic and widespread strain gradient exists along the radius of nanoparticles [36, 37, 38, 39, 40, 41, 42]. According to *Yuheng Zhang effect* and *Yuheng Zhang equation* [5, 6], this strain gradient in the nanoparticles may give rise to a corresponding electric field along their radius, and it is [43]

$$\vec{E}_n = \frac{\partial E_F}{e\partial \xi_{ij}} \nabla \xi_{ij} \tag{25}$$

where ξ_{ij} is the strain components. For a nanoparticle with radius several nanometers, the internal radial electric field may approach the magnitude $\sim 10^8$ V/m. Hence, a noticeable charge separation may appear in the nanoparticle and a larger number of charges could accumulate at the nanoparticle surfaces. For simplicity, this electric field is assumed to be a constant and the charge density distribution within the metal nanoparticles may be approximated as that in the core of the earth [44]

$$\rho(r) = 2D/r - D\delta(r - r_0) \tag{26}$$

where r_0 is the radius of the metal nanoparticle, $\rho(r)$ is radius dependence of charge density, the parameter is electric displacement $D=\varepsilon_0 \varepsilon E_n$ and its magnitude may reach a value 10 C/m^2 for some metal nanoparticles. Analogous to the possible creation of the earth's geomagnetic field [44], fast rotation of such a metal nanoparticle from west to east (the same rotational direction as the earth) will generate a correlated magnetic field which may be described in cylindrical coordinate system shown in Figure 8 by

$$
\begin{aligned}
B_r &= -\pi \frac{\mu_0 D}{2T} \frac{r_0^4}{R^3} sin2\psi \quad (R > r_0) \\
B_\varphi &= 0 \\
B_z &= -\frac{\pi}{3} \frac{\mu_0 D}{2T} \frac{r_0^4}{R^3} (1 + 3\cos 2\psi) \quad (R > r_0)
\end{aligned} \tag{27}
$$

where R is the distance from center of the metal nanoparticle, T the period of rotation, μ_0 the magnetic susceptibility outside the nanoparticle, ψ the polar angle from positive z-axis, φ the azimuthal angle in the x-y plane from the x-axis .

Displayed by these equations is that the yielded magnetic field is a magnetic dipole field. For a metal nanoparticle with an average radius 2 *nm*, if the period of its fast rotation could be 1 *ps*, a magnetic dipole field may be created around the nanoparticle and the field strength at the equator may reach ~200 *Gauss*. Of emphasized here is that the electric field along the radius of metal nanoparticles was assumed to be a constant, but the actual electric displacement may not be a constant and varies with position. So the above calculations mainly predict the mechanism of magnetic field yielded by the fast rotation of a metal nanoparticle and a more precise determination of the magnetic field still depends on a more precise position dependence of electric displacement vector.

In spite of the remarkable size difference between the metal nanoparticle and the earth, fast rotation of a metal nanoparticle may be very like the earth considering the following points. First, a notable charge separation exists along radius for both the metal nanoparticle and the metallic core of the earth because of *Yuheng Zhang effect*. Second, according to the possible mechanism of the earth's geomagnetic field [44], fast rotation of both the metal nanoparticle and the earth could generate a magnetic

dipole field around them. Taking these similarities into account, the rotating metal nanoparticle may be named as "micro-earth". How can people give birth to such a fast rotated micro-earth? One possible method might employ the incidence of photons with angular momentum. The effective transfer of the angular momentum of photons to a nanoparticle may enable it to rotate rapidly and yield a micro-earth. In the future, the micro-earth may be utilized in some important areas such as micro-detection and so on.

2.8 Modification on molecular orbital of adsorbed molecules

As indicated in the previous section, the popular strain gradient in nanoparticles usually generate a noticeable charge separation and the charges may agglomerate at surfaces especially sharp edges and correlated corners as shown in Figure 9. As a result, an intense electrostatic field may be created close to the nanoparticle surface. The field may sensitively dependent on position and decay rapidly with distance away from the surface. In general, the spatial distribution of the electrostatic field may exhibit the following properties

$$\begin{aligned} E(r) &\propto \frac{1}{r^2} \quad (r < l_0); \\ E(r) &\propto \frac{1}{r^3} \quad (l_0 < r < 2R_0); \\ E(r) &\propto \frac{1}{r^4} \quad (2R_0 < r); \end{aligned} \tag{28}$$

where r is distance of molecules from the nanoparticle surface, l_0 denotes the surface strain relaxation length and is usually the length of several atomic layers ~1 *nm* [42, 45, 46], R_0 the radius of the nanoparticle. This electrostatic field may approach a magnitude ~10^8 *V*/*m* for molecules adsorbed on the surface and even reach ~10^9 *V*/*m*

near the sharp edges and corners. To be anticipated, this field may give rise to modifications on molecular structure of adsorbed molecules. To show this effect and for clarity in physics, the simplest Hamiltonian for an electron with two-orbital basis is taken

$$H_0 = E_a|a\rangle\langle a| + E_b|b\rangle\langle b| + V|a\rangle\langle b| + V^\dagger|b\rangle\langle a| \tag{29}$$

where E_a, E_b are the eigenenergy for the two electron orbitals, $|a\rangle$, $|b\rangle$ are Dirac bras for the two electron orbitals, V the orbital overlap energy. The electrostatic field may induce other off-diagonal matrix elements such as $\left\langle e\vec{E}\cdot\vec{r}\right\rangle_{ab}|a\rangle\langle b|$ and $\left\langle e\vec{E}\cdot\vec{r}\right\rangle_{ba}|b\rangle\langle a|$. Here their related diagonal matrix elements are ignored, because they may be much smaller than the eigenenergy E_a, E_b for the two electron orbitals. The total Hamiltonian may be

$$H = E_a|a\rangle\langle a| + E_b|b\rangle\langle b| + V|a\rangle\langle b| + V^\dagger|b\rangle\langle a| + \left\langle e\vec{E}\cdot\vec{r}\right\rangle_{ab}|a\rangle\langle b| + \left\langle e\vec{E}\cdot\vec{r}\right\rangle_{ba}|b\rangle\langle a| \tag{30}$$

where the terms are $\langle\ \rangle_{ab} = \langle a|\ |b\rangle$ and $\langle\ \rangle_{ba} = \langle b|\ |a\rangle$. For covalent bonds where the relation $|E_a - E_b| << |V|$ exists, the resultant solution for the total Hamiltonian may be obtained

$$E_\pm \approx \frac{E_a + E_b}{2} \pm \left|V + \left\langle e\vec{E}\cdot\vec{r}\right\rangle_{ab}\right| \left[1 + \frac{(E_a - E_b)^2}{8\left|V + \left\langle e\vec{E}\cdot\vec{r}\right\rangle_{ab}\right|^2}\right] \tag{31}$$

As is seen clearly, the covalent bond strength may be modified by the electrostatic field, and a larger field usually causes a more notable modification. A field with magnitude ~10^9 *V/m* may lead to an energy shift ~0.1 *eV*. Hence, the electric structure of molecules physically adsorbed at surface of nanoparticles may often be altered to some extent, which may bring some shifts for the related fluorescence, infrared

spectroscopy, Raman spectroscopy and nuclear magnetic resonance (NMR) spectroscopy. The spectrum shift of the molecules may vary with distance and could approach several percent for these molecules adsorbed at nanoparticle surfaces. Besides, the electrostatic field in the vicinity of nanoparticles may display remarkable electric quadrupole field which may influence selection rules for related spectrum.

2.9 Quenching of fluorescence

Because of charge separation and accumulation of net charges at metallic nanoparticle surface shown in Figure 9, an ultra-strong electric field may be yielded and applied to the nearby molecules. Thus a correlated electrostatic dipole may be generated in the molecule, and a strong static dipole-dipole interaction (SDD) may appear between the metallic nanoparticle and the adjacent molecules. The Hamiltonian may be written as

$$H_{dd} \approx \frac{1}{4\pi\varepsilon_0}\sum_i\left[\frac{\vec{P}_e\cdot\vec{p}_i(\vec{r}_i)}{|\vec{r}_i|^3}-\frac{3\left(\vec{P}_e\cdot\vec{r}_i\right)\left(\vec{p}_i(\vec{r}_i)\cdot\vec{r}_i\right)}{|\vec{r}_i|^5}\right] \tag{32}$$

where P_e is the near field electric dipole moment at the nanoparticle and it may be proportional to the internal electric field along the radius in the nanoparticle $P_e \propto \alpha_n(0)E$, α_n the electrostatic polarizability of nanoparticle, $p_i(r_i)$ denotes the electric dipole moment for a molecule at position r_i and it may sensitively depend on the local electrostatic field $E(r_i)$ exerted by the adjacent nanoparticle, ε_0 the vacuum permittivity.

This SDD may exhibits several typical properties. First, it may be a near field interaction. It can be very strong within a small scale ($r \sim l_0$) and the strength may be

$H_{dd} \propto \alpha_n(0) E_n \alpha_m(0) E(r_i)$ where $\alpha_m(0)$ represents the electrostatic polarizability of the molecules at position r_i, respectively. Second, it sensitively relies on the electrostatic polarizability of nanoparticle α_n and a bigger polarizability usually can not only give birth to a larger near field electric dipole moment at the nanoparticle but also cause a much more intense electrostatic field around the nanoparticle. The static polarizability of metals may be large and be proportional to square of the phenomenological relaxation time τ of electrons $\alpha_n(0) \propto (\omega_p \tau)^2$ [28, 47] where ω_p is the plasma frequency. Besides, the electron relaxation time τ is usually proportional to the static electrical conductivity $\sigma(0)$ so that the relation exists $\alpha_n(0) \propto [\sigma(0)]^2$. Considering that the electrostatic field $E(r_i)$ around the metallic nanoparticle may linearly depend on the amount of separated net charges in the nanoparticle, the strength of SDD interaction may be proportional to the square of static polarizability $H_{dd} \propto [\alpha_n(0)]^2$. Therefore, the strength of SDD interaction may be $H_{dd} \propto [\sigma(0)]^4$, meaning that the metallic nanoparticles especially those with much higher static electrical conductivity $\sigma(0)$ may usually result in a stronger SDD interaction. Third, the SDD interaction may decay very quickly with increasing distance, as may be ascribed to two main factors. One is the fast attenuation of local electrostatic field $E(r_i)$ applied on the molecule, which may reduce the electric dipole moment $p_i(r_i)$ for a molecule. The other is natural attenuation of the SDD interaction with distance as shown by the above equation. Hence, the distance dependence of the SDD may be

$$
\begin{aligned}
H_{dd} &\propto \frac{1}{r^5} \quad (r < l_0); \\
H_{dd} &\propto \frac{1}{r^6} \quad (l_0 < r < 2R_0); \\
H_{dd} &\propto \frac{1}{r^7} \quad (2R_0 < r);
\end{aligned}
\tag{33}
$$

This near field SDD interaction may be very strong and play a key role for the quenching of fluorescence. The related quantum mechanism may be illustrated in Figure 10. When a beam of laser is incident on the molecules, the electrons in the molecular ground state would hop to excited states in terms of absorbing energy-matched photons shown in Figure 10(a). The related quantum transition may be a one-photon process and be described well by Fermi golden rule [47],

$$
W_{f\leftarrow i} = \frac{2\pi}{\hbar}\left|\left\langle \psi_e \left| \frac{eE_0}{m_e\omega} e^{i\vec{k}\cdot\vec{r}}\vec{e}\cdot\vec{p} \right| \psi_g \right\rangle\right|^2 \delta\left(\varepsilon_{me} - \varepsilon_{mg} - \hbar\omega\right) \tag{34}
$$

where $W_{f\leftarrow i}$ is the quantum transition rate from the ground state $|\psi_g\rangle$ to the excited state $|\psi_e\rangle$, $\vec{e}$ the polarization unit vector of incident laser beam, E_0 the magnitude of electric field of the laser, $\vec{p}$ the momentum operator, ε_{me}, ε_{mg} the ground state energy and excited state energy of the electron belonging to the related molecules, respectively, $\hbar$ the reduced Plank constant.

The excited electron energy may be subsequently transferred to the adjacent nanoparticles quickly by the strong SDD interaction between nanoparticles and the related molecules as shown in Figure 10(b). This energy transferring process conforms to energy conservation, so it could be regarded an electron double-dipole resonance (EDDR). The quantum transition rate may be determined by the SDD interaction and also be described by Fermi-golden rule [47],

$$W_{EDDR} = \frac{2\pi}{\hbar} \sum_{\varphi_e, \varphi_g} \left| \left\langle \varphi_e \left| \left\langle \psi_g \left| H_{dd} \right| \psi_e \right\rangle \right| \varphi_g \right\rangle \right|^2 \delta\left[\varepsilon_{me} + \varepsilon_g - \varepsilon_{mg} - \varepsilon_e \right] \qquad (35)$$

where W_{EDDR} is the quantum transition rate caused by EDDR, $|\varphi_g\rangle$, $|\varphi_e\rangle$ the ground state and excited state wave functions of electron in the nanoparticle.

This EDDR may display some unique characteristics. First, it is a physical process and may not associate with charge transfer between the nanoparticle and adsorbed molecules. So the EDDR may not bring alterations in molecular bonds for the related adsorbed molecules. Second, the EDDR may be suitable for arbitrary electron energy transfer and thereby it might be widespread in various physical systems. Owing to the strong SDD interaction, the quantum transition rate stemming from EDDR may far exceed that for the fluorescence emission. Hence, most of the photon energy absorbed by electrons in the molecules may be fast transferred to the electrons in the neighbor nanoparticles so that the fluorescence emission of molecules would be suppressed greatly.

According to this EDDR mechanism, the quenching of fluorescence may be dominated by several vital factors. One is the distance between the nanoparticle and molecules. And a smaller distance usually leads to a stronger SDD interaction and EDDR, which inversely quenches the fluorescence more seriously. Another one is the polarizability of nanoparticle. Generally speaking, metallic nanoparticles with higher electric conductivity $\sigma(0)$ usually possess a larger electrostatic polarizability, thereby yielding a stronger SDD interaction and EDDR, *i.e.*, $H_{dd} \propto [\sigma(0)]^4$. Therefore, the existence of metallic nanoparticles such as Ag, Au and Cu nanoparticles with good electric conductivity would be anticipated to lead to obvious quenching of

fluorescence, which was verified by experimental results [48, 49]. The third one is the relaxation strain and the mechanical-electric coupling strength of the metallic nanoparticle. A larger surface relaxation strain and mechanical-electric coupling strength may induce a stronger SDD interaction and EDDR, which may suppress the fluorescence emission of neighbor molecules more effectively. The fourth one may be the temperature. As temperature decreases, the electric conductivity of metals usually increases gradually, which may enhance the SDD interaction and EDDR, resulting in a more severe quenching of fluorescence for the neighboring molecules.

2.10 Surface enhanced Raman scattering (SERS)

SERS was first observed in 1970s [50, 51, 52] and it could be utilized as a ultra-sensitive analytical technique to detect minor amount of molecules in terms of the fingerprint Raman spectrum. Since its discovery, it has attracted worldwide attention and has brought several tens of thousands of publications in which several recent reviews have given excellent introduction and summaries [53, 54, 55]. For the scientific origin of SERS, much theoretical attempts has been made to understand various experimental phenomena on SERS since the discovery of SERS. By means of worldwide research in recent several decades, it is popularly believed to originate from two mechanisms. One is the electromagnetic enhancement associated with surface plasma excitations, which is usually regarded as the main mechanism of SERS [53, 54, 55]. The other is chemical enhancement resulting from charge transfers between the metal nanoparticles and adsorbed target molecules [53, 54, 55]. Despite that these theoretical models could capture some physics on SERS, no model could

clarify all the important phenomena revealed by various SERS experiments. So, for the further development and wide applications of SERS in multi-fields, constructing a unified theoretical model for SERS may be very necessary, but it is very challenging and still an open topic [53, 54, 55].

Upon SERS, a successful model must answer the questions below,

1) Why does the Raman band shift in the SERS experiments?
2) What are the reasons for the Raman band fluctuations?
3) Why does the externally applied voltage influence the Raman intensity?
4) Why do the semiconductor nanoparticles generate SERS?
5) Why can the sharp surface features such as sharp edges, corners and nano-stars yield notable SERS?
6) Why can the SERS yield so large an enhanced factor (EF)?
7) Why can hot spots enhance the EF?
8) What is the physical mechanism for distance dependence of SERS?
9) Why does the SERS sensitively depend on frequency of incident laser?
10) What are the selection rules for the SERS?

In this section, by employing the discovered strong electrostatic field, related SDD and the resultant EDDR between nanoparticles and neighboring molecules, a new physical mechanism for the SERS was proposed and utilized to understand the vital phenomena on SERS.

By means of quantum second-order perturbations [47], considering single quantum excitation in the nanoparticle (the quantum excitation in metal nanoparticles may be

the excitation of the localized surface plasmon, but it may be the creation of electron-hole pair in semiconductors) and the EDDR between nanoparticle and adsorbed molecules as shown in Figure 11, the quantum transition coefficient from the ground state to the intermediate virtual state of electron in a molecule may be given by

$$C_{i\leftarrow g}\left(\vec{q},\omega\right)=\frac{eE_0}{im_e\omega}\sum_{\varphi_e,\varphi_g}\frac{\left\langle\varphi_g\left|\left\langle\psi_i\left|H_{dd}\right|\psi_g\right\rangle\right|\varphi_e\right\rangle\left\langle\varphi_e\left|e^{i\vec{q}\cdot\vec{r}}\vec{e}\cdot\vec{p}\right|\varphi_g\right\rangle}{\left(\varepsilon_{mg}-\varepsilon_{mi}+\hbar\omega+i\eta\right)\left(\varepsilon_g-\varepsilon_e+\hbar\omega+i\eta\right)} \tag{36}$$

where $C_i(q, \omega)$ is the wavevector q and angular frequency ω dependence of quantum transition coefficient, m_e the electron mass, E_0 the magnitude of electric field of the laser, $\vec{e}$ the polarization unit vector of incident laser beam, $\vec{p}$ the momentum operator, $\hbar$ the reduced Plank constant, $|\varphi_e>$, $|\varphi_g>$ present the ground state wave function and electronic excited state wave function in nanoparticles, ε_e, ε_g the corresponding eigenenergy for the states, $|\psi_i>$, $|\psi_g>$ the intermediate virtual state and ground state of electron in the molecules, ε_{mi}, ε_{mg} denote the corresponding energy levels for the intermediate state and ground state, respectively.

This quantum transition coefficient may determine the pumping process of SERS and the related EF.

The radiated power of Raman scattering may be given by [54, 56]

$$P_{Raman}=\frac{\left(\omega\pm\omega_q\right)^4}{12\pi\varepsilon_0}\left|\vec{P}\left(\omega\pm\omega_q\right)\right|^2 \tag{37}$$

where ω_q is the frequency of molecular vibration mode, ε_0 the vacuum permittivity, $P(\omega\pm\omega_q)$ the oscillating electric dipole of the molecules. Combining quantum transition coefficient from ground state to the intermediate virtual state and the power

of Raman scattering, one may obtain

$$P_{SERS} \propto \frac{\left(\omega \pm \omega_q\right)^4 \left(n_q + \frac{1}{2} \mp \frac{1}{2}\right)}{12\pi\varepsilon_0} E_0^2 \sum_{\gamma\rho} \left|\alpha_{\gamma\rho}^{SERS}\right|^2 \tag{38}$$

$$\alpha_{\mu\nu}^{SERS} = \sum_{\varphi_e,\varphi_g}^{\psi_i,\psi_g} \frac{\left\langle \varphi_g \middle| \left\langle \psi_i \middle| H_{dd} \middle| \psi_g \right\rangle \middle| \varphi_e \right\rangle \left\langle \varphi_e \middle| \mu'_\mu \middle| \varphi_g \right\rangle \left\langle \psi_g \middle| \mu_\nu \middle| \psi_i \right\rangle}{\left(\varepsilon_{mg} - \varepsilon_{mi} + \hbar\omega + i\eta\right)\left(\varepsilon_g - \varepsilon_e + \hbar\omega + i\eta\right)} \tag{39}$$

where n_q is the number of molecular vibrations, $\alpha_{\mu\nu}^{SERS}$ is the component of effective polarizability tensor for SERS, the subscripts μ and ν are the incident photon polarization direction and scattered photon polarization direction in cartesian coordinates (x, y, z), μ is the Stokes (anti-Stokes) dipole moment operator for the molecules, μ' the dipole moment operator for the nanoparticle. This effective polarization tensor determines the selection rules for SERS.

So the single-molecule EF (SMEF) of SERS could be estimated by

$$EF_{sm}\left(\vec{k},\omega\right) \approx \left|\frac{l_0^3}{\left(2\pi\right)^2 r_i^3} \varepsilon_{n2}\left(\vec{k},\omega\right)\right|^2 \left|\frac{\alpha_n(0)E_n}{\alpha_n\left(\vec{k},\omega\right)E_0} \frac{\alpha_m(0)E\left(r_i\right)}{\alpha_m\left(\vec{k},\omega\right)E_0}\right|^2 \tag{40}$$

where $\alpha_n(k,\omega)$, $\alpha_m(k,\omega)$ are the momentum vector k and angular frequency ω dependence of polarizability of nanoparticles and molecules, respectively, $\alpha_n(0)$, $\alpha_m(0)$ the electrostatic polarizability of nanoparticles and molecules, $\varepsilon_{n2}(k,\omega)$ the imaginary part of relative dielectric constant of nanoparticles, E_n the electrostatic field in the nanoparticle due to surface strain relaxation and $E(r_i)$ the position r_i dependence of electrostatic field experienced by the molecule.

Equation (40) shows that the SMEF strongly depends on the distance between the nanoparticle and the molecules. Based on the distance dependence of SDD magnitude shown in Equations (28) and (33), the overall $EF(k,\omega)$ may be $EF_{sm}(k,\omega)4\pi(R_0+r)^2$,

thus

$$EF\left(\vec{k},\omega\right) \propto \frac{\left(R_0+r\right)^2}{r^{10}} \quad \left(r < l_0\right);$$
$$EF\left(\vec{k},\omega\right) \propto \frac{\left(R_0+r\right)^2}{r^{12}} \quad \left(l_0 < r < 2R_0\right); \tag{41}$$
$$EF\left(\vec{k},\omega\right) \propto \frac{\left(R_0+r\right)^2}{r^{14}} \quad \left(2R_0 < r\right);$$

Since the radius R_0 of utilized nanoparticle is usually much larger than surface relaxation length l_0, *i.e.*, $R_0 >> l_0$, hence, the overall $EF(k,\omega)$ may decay with r^{-10} in the near field range $r<l_0$, which was verified by experimental observations [57].

As indicated by Equation (40), the EF of SERS may obviously depend on the frequency (wavelength) of incident light. The imaginary part of relative dielectric function of a system is proportional to its absorption coefficient [28, 47], so the EF of SERS may reach its peak value when the frequency (wavelength) of light is coincident with the characteristic frequency (wavelength) of maximum absorption coefficient of nanoparticle, which is the commonly observed experimental results [58, 59].

Also shown by this equation is that not only metal nanoparticles but also semiconductor nanoparticles possessing both large static polarizability $\alpha_n(0)$ and imaginary part of dynamic polarizability $\varepsilon_{2n}(\omega)$ may give birth to a noticeable SERS as well, which was verified by experimental observations [60, 61].

Based on Equations (40), one may understand the vital role of sharp surface features in the SERS. Sharp surface features such as nano-star, sharp edges and corners mean that there exist many regions with dramatic strain relaxation which may further generate a strong electrostatic field and apparent net charge accumulation in

these regions according to *Yuheng Zhang equation*. The net charges at sharp edges and corners will yield an intensely electrostatic field and thereby cause a strong SDD interaction between neighboring molecules and surface regions with sharp features, as may result in notable SERS. So the regions close to the sharp edges and corners may behave as the active spots for SERS and the size of these active spots may be the order of the surface relaxation length l_0, *i.e*, several atomic layers ~1 *nm* [42, 45, 46]. For the nanoparticle agglomeration systems, the electrostatic field in the nano-gap between two nanoparticles may be greatly enhanced due to the mutual induced more charges at confronting side of the other nanoparticle. Therefore, the SDD and EDDR between nanoparticles and molecules in the nano-gap may be conspicuously enhanced, leading to a more notable SERS. The regions in the nano-gap may be the hotspots already revealed in many experiments [55, 62]. Based on the nanometer sized surface relaxation length l_0, the hotspot size may be ~1 nm, which is in accord with experimental results [55, 62, 63].

As stated in previous section, the intense electrostatic field generated by surface sharp features such as sharp edges and corners would bring alterations in covalent bond strength of molecules, thereby resulting in the Raman band shift for the nearby molecules especially those adsorbed at positions with surface sharp features. In terms of a simple estimation, the largest shift of Raman band may reach several percent, and as a rule a bigger shift usually corresponds to a larger single-molecule EF of SERS owing to a stronger SDD interaction and EDDR. In the SERS experiments, due to the randomness and disorder of sharp features at nanoparticle surfaces, the yielded

electrostatic field may also exhibit complexity which may subsequently induce a distinct Raman shift, Raman intensity, spectral shape and EF of SERS in different experiments even with the same type of nanoparticles as the SERS substrate. This may be confirmed by the commonly encountered experimental observations on the SERS fluctuations such as intensity fluctuation, spectral shape fluctuation, Raman peak position fluctuation and Raman peak width fluctuation [64].

In previous investigations, the experimental observations that SERS intensity relies on electrochemical potential of substrate was recognized as a strong evidence for the chemical enhancement mechanism dominated by charge transfer between SERS substrate and adsorbed molecules [55]. However, a quite different and complete physical mechanism for the effect of electrochemical potential on SERS may be put forward here. An externally applied electric voltage on the SERS substrate would change the electrostatic field felt by the adsorbed molecules, so that both the SDD interaction and EDDR may be greatly altered, which may further result in obvious variations of SERS intensity. A simple comparison between this mechanism and chemical enhancement could be performed. Chemical enhancement requires charge transfer, but the EDDR mechanism may require charge separation induced by strains at sharp surface features. Chemical enhancement occurs only for the chemically adsorbed molecules, but the EDDR mechanism may be valid for molecules several nanometers away. Discovery of so-called shell-isolated nanoparticle-enhanced Raman spectroscopy (SHINERS) where the metal nanoparticles were coated by ultrathin semiconductor films [55, 65, 66] preventing direct interaction between nanoparticles

and adsorbates may disagree with the chemical enhancement mechanism, but might be consistent with EDDR mechanism.

The selection rules of SERS may be altered by the EDDR between SERS substrate and the adsorbed molecules as indicated by Equations (32) and (39). In the equations, the amplitude of the diagonal terms $\langle\varphi_g|P_{e\gamma}|\varphi_e\rangle\langle\varphi_e|\mu'_\mu|\varphi_g\rangle$ (μ=γ), $\langle\psi_i|p_{i\rho}(\vec{r}_i)|\psi_g\rangle\langle\psi_g|\mu_\nu|\psi_i\rangle$ (ν=ρ) may be much larger than other off-diagonal terms $\langle\varphi_g|P_{e\gamma}|\varphi_e\rangle\langle\varphi_e|\mu'_\mu|\varphi_g\rangle$ ($\mu\neq\gamma$), $\langle\psi_i|\vec{p}_{i\rho}(\vec{r}_i)|\psi_g\rangle\langle\psi_g|\mu_\nu|\psi_i\rangle$ ($\nu\neq\rho$), thus these approximations may be appropriate,

$$\begin{aligned}\langle\varphi_g|P_{e\gamma}|\varphi_e\rangle\langle\varphi_e|\mu'_\mu|\varphi_g\rangle &\propto \delta_{\mu\gamma}\\ \langle\psi_i|p_{i\rho}(\vec{r}_i)|\psi_g\rangle\langle\psi_g|\mu_\nu|\psi_i\rangle &\propto \delta_{\nu\rho}\end{aligned} \tag{42}$$

where the Kronecker symbol is $\delta_{\mu\gamma}$=1 for the case μ=γ, otherwise it is zero. These approximations may be applicable for the nanoparticles and molecules without off-diagonal terms in their respective polarizability tensors. So the effective polarizability tensor for SERS may be given by

$$\alpha_{\mu\nu}^{SERS}=\sum_{\varphi_e,\varphi_g}^{\psi_i,\psi_g}\frac{\langle\varphi_g|P_{e\mu}|\varphi_e\rangle\langle\varphi_e|\mu'_\mu|\varphi_g\rangle\langle\psi_g|\mu_\nu|\psi_i\rangle\langle\psi_i|p_{i\nu}(\vec{r}_i)|\psi_g\rangle}{(\varepsilon_{mg}-\varepsilon_{mi}+\hbar\omega+i\eta)(\varepsilon_g-\varepsilon_e+\hbar\omega+i\eta)}\frac{1}{4\pi\varepsilon_0}\sum_i\left(\frac{\delta_{\mu\nu}}{|\vec{r}_i|^3}-\frac{3r_{i\mu}r_{i\nu}}{|\vec{r}_i|^5}\right) \tag{43}$$

This equation displays that the effective polarizability tensor for SERS showing molecule position dependence may determine the selection rules of SERS. Some normal Raman-active vibration mode may be silent when the molecules at positions fulfill the conditions $3r_{i\mu}r_{i\mu}=(r_i)^2$. Furthermore, it may reveal that the TEF at the surface of metal nanoparticles can give rise to additional contributions to Raman scattering, *i.e.*, the off-diagonal term in the round brackets in Equation (43), as could activate forbidden vibration mode in the common Raman scattering. It may be the

physical origin of popular experimental observations of forbidden Raman mode in SERS [67, 68, 69].

To examine whether this EDDR mechanism grasp the physics of SERS or not, the magnitude of SMEF should be estimated. As the analysis in the previous section of Micro-earth, the electrostatic field within the strain relaxation length of nanoparticle may reach a magnitude ~10^8 *V*/*m*, and the field $E(r_i)$ applied on the adsorbed molecules especially these at the edges and corners may be in the range 10^8~10^9 *V*/*m*. The electric field E_0 of the incident laser in the experiments was usually ~10^6 *V*/*m* corresponding to a laser radiation power density ~10^5 *W*/*cm*^{2} [67, 68]. In the cases that the metal nanoparticles were used as SERS substrate, inserting the relative dielectric function of metals [28, 47], the SMEF could be written as

$$EF_{sm}\left(\vec{k},\omega\right)\approx\left|\frac{l_0^3}{\left(2\pi\right)^2 r_i^3}\frac{\sigma(0)}{\varepsilon_0\omega}\right|^2\left|\frac{E_n}{E_0}\frac{\alpha_m(0)E(r_i)}{\alpha_m\left(\vec{k},\omega\right)E_0}\right|^2 \tag{44}$$

where $\sigma(0)$ is the static electrical conductivity of the metal, ε_0 the vacuum permittivity. If the electrostatic polarizability of molecules is comparable to its dynamic polarizability, the optimum SMEF using metal nanoparticles Ag, Au and Cu as SERS substrate could be estimated to reach a value as high as 10^8~10^{10}, which agrees with conclusions [54, 55] obtained from many experimental observations.

Meanwhile, the yielded electric field on molecules $E(r_i)$ may be proportional to the amount of separated charges in the metal nanoparticle. The amount of separated charges is usually proportional to the static polarizability, so the field $E(r_i)$ may be proportional to the static polarizability of metal nanoparticle, i.e., $E(r_i)\propto\alpha_n(0)$.

Furthermore, according to static conductivity and relative dielectric function of metals [28, 47], the relation between static polarizability and static conductivity of metals exists $\alpha_n(0)\approx[\sigma(0)]^2/\varepsilon_0\omega_p^2$. Therefore, the SMEF employing metal nanoparticles as SERS substrate may follows the relation $EF_{sm}(k,\ \omega)\propto[\sigma(0)]^6/(\varepsilon_0\omega_p^2)^2$. On the other hand, the electric field in the strain relaxation length l_0 remarkably relies on the mechanical-electric coupling strength and the surface strain of the nanoparticles. Combining these factors, the following relation may be valid for SMEF by means of metal substrate,

$$EF_{sm}\left(\vec{k},\omega\right)\propto\frac{\left[\sigma\left(0\right)\right]^6}{\left(\varepsilon_0\omega_p^2\right)^2}\left|\frac{\partial E_F}{e\partial\xi_{ij}}\xi_{ij}\right|^4 \tag{42}$$

As shown, the SMEF depends on electric conductivity $\sigma(0)$, mechanical-electric coupling strength $\left|\partial E_F/e\partial\xi_{ij}\right|$ and the surface strains ξ_{ij}. Hence, the metal nanoparticles such as Ag, Au and Cu exhibiting much higher electrical conductivity than other transition metals can usually result in much stronger SERS，which was the experimental observations [70, 71, 72, 73].

As indicated by the above analysis, the proposed simple mechanism based on EDDR between SERS substrate and neighboring molecules may grasp the physics of SERS and could help people understand the complex phenomena on SERS deeply.

The important role of EDDR has been discussed for the suppression of fluorescence and SERS in this work. Of emphasized is that the EDDR may be a highly-efficient energy transfer channel between nanoparticles and their nearby systems such as nanoparticles, molecules and so on. To be anticipated, it may also play a key role in

other fields such as tip-enhanced Raman scattering (TERS), nanoparticle-assisted photocatalysis and so on.

3. Conclusion

In summary, the TEF at metal surfaces and its important effects in some distinct areas may be unraveled in this work. It was found that TEF may have a vital effect on photoelectron emission spectroscopy, redistribution of minority atoms, Reshba effectand so on. On the other hand, the electrostatic field at the nanoparticle surfaces may lead to the discovery of the EDDR. To be excited, using EDDR a simple unified theoretical model for SERS, a longstanding problem in physics and chemistry, may be constructed here. This model may capture the main physics of SERS through the analysis of experimental phenomena on SERS. Overall, the discovered TEF at metal surface may help people to investigate the related mechanical, physical and chemical effects, and it may find important applications in various areas in the future.

References

[1] Richard Feynman, Robert B. Leighton, Matthew L. Sands, The Feynman Lectures on Physics, vol.2, Pearson Education, Inc., Publishing as Prentice Hall, Inc. 2004, pp.4-1, pp.5-8.

[2]Gerald L. Pollack, Daniel R. Stump, Electromagnetism, Pearson Education, Inc., Publishing as Addison Wesley, 1st edition, 2002, pp.94.

[3] David K. Cheng, Field and Wave Electromagnetics, Pearson Education, Inc., Publishing as Addison Wesley, 2nd edition, 1989, pp.101-102.

[4] Shuohong Guo, Electrodynamics, 3rd edition, Beijing: Higher Education Press, 2008, pp.37, pp.40.

[5] Yuanjie Huang, Strain-Induced Electric Effect in Metals, Journal of Materials Sciences and Applications, **5**(3), 58-62(2019).

[6] Yuanjie Huang, Strain Induced Electric Effect in Condensed Matters, Journal of Materials Sciences and Applications, **5**(3), 44-57(2019).

[7] Yuanjie Huang, Electric features of dislocations and electric force between dislocations, Math. Mech. Sol., V. **26**(4), 616-628 (2021).

[8] J. F. Freedman, Residual Stress in Single-Crystal Nickel Films, IBM Journal of Research and Development, V. **6**(4), 449-455(1962).

[9] Ame´lie Moranc¸ais, Mathieu Fe`vre, Manuel Franc¸ois, Nicolas Guel, Serge Kruch, Pascale Kanoute, Arnaud Longuet, Residual stress determination in a shot-peened nickel-based single-crystal superalloy using X-ray diffraction, J. Appl. Cryst., V. **48**, 1761–1776(2015).

[10] F. Bechstedt, Principles of Surface Physics, Springer-Verlag Berlin Heidelberg, 2003, pp.293-315.

[11] B. A. Rose, Measurements on contact potential difference between different faces of copper single crystals, Phys. Rev., V. **44**, 585 (1933).

[12] J. C. Rivière, Contact potential difference measurements by the Kelvin method, Proc. Phys. Soc. B V. **70**(7), 676 (1957).

[13] N. A. Robertson, J. R. Blackwood, S. Buchman, R. L. Byer, J. Camp, D. Gill, J. Hanson, S. Williams, P. Zhou, Kelvin probe measurements: investigations of the patch effect with applications to ST-7 and LISA, Class. Quantum Grav., V. **23**, 2665–2680(2006).

[14] Rashba E. I., Symmetry of energy bands in crystals of wurtzite type: I. symmetry of bands disregarding spin-orbit interaction Sov. Phys.-Solid State, V. **1**, 368–80(1959).

[15] Bychkov Y. A., Rashba E. I., Properties of a 2D electron gas with lifted spectral degeneracy. JETP Lett., V. **39**, 66-69(1984).

[16] D. Stein, K. v. Klitzing, G. Weimann, Electron Spin Resonance on GaAs-$Al_xGa1\text{-}_xAs$ Heterostructures, Phys. Rev. Lett., V. **51**(2), 130-133(1983).

[17] Hans Lüth, Solid Surfaces, Interfaces and Thin Films, 5th edition, Springer Berlin Heidelberg, 2010, pp.263-276.

[18] Li-na Zhu, Bin-shi Xu, Hai-dou Wang, Cheng-biao Wang, Effect of residual stress on the nanoindentation response of (100) copper single crystal, Materials Chemistry and Physics, V. **136**, 561-565(2012).

[19] D.Y. Jang, T.R. Watkins, K.J. Kozaczek, CR. Hubbard, O.B. Cavin, Surface residual stresses in machined austenitic stainless steel, Wear, V. **194**, 168-173 (1996).

[20] C. Shet, X. Deng, Residual stresses and strains in orthogonal metal cutting, International Journal of Machine Tools & Manufacture, V. **43**, 573–587(2003).

[21] Andrea Damascelli, Zahid Hussain, Zhi-Xun Shen, Angle-resolved Photoemission studies of the cuprate superconductors, Rev. Mod. Phys., V. **75**(2), 473-541(2003).

[22] E. Pavarini, E. Koch, J. van den Brink, G. Sawatzky (eds.) Quantum Materials: Experiments and Theory Modeling and Simulation Vol. 6, Forschungszentrum Jülich, 2016, pp.14.2

[23] Harold J.W. Zandvliet and Arie van Houselt, Scanning Tunneling Spectroscopy, Annual Rev. Anal. Chem., V. **2**, 37-55(2009).

[24] J. Tersoff, D. R. Hamann, Theory of The Scanning Tunneling Microscope, Phys. Rev. B V. **31**(2), 805-813(1985).

[25] R. J. de Vries, A. Saedi, D. Kockmann, A. van Houselt,a_ B. Poelsema, and H. J. W. Zandvliet, Spatial mapping of the inverse decay length using scanning tunneling microscopy, Appl. Phys. Lett., V. **92**, 174101(1-3)(2008).

[26] R. M. Feenstra, J. A. Stroscio, A. P. Fein, Tunneling spectroscopy of the Si (111) 2× 1 surface, Surface science, V. **181**, 295-306(1987)

[27] Yuanjie Huang, Discovery of A New Transport Mechanism and Physical Origin of Hume-Rothery Rules, viXra:1902.0264 .

[28] Shouheng Yan, Fundamentals of Solid State Physics, 3rd edition, Beijing: Beijing

University Press, 2011, pp.19-20, pp.188-189.

[29] T. Teorell. *Studies on the "diffusion effect" upon ionic distribution–I Some theoretical considerations*. Proc. N. A. S. USA, V. **21**, 152–161(1935).

[30] H. Okamoto, M.E. Schlesinger, E.M. Mueller, ASM Handbook Volume 3: Alloy Phase Diagrams, **ASM** International, 2016.

[31] Lingxuan Peng, Emilie Ringe, Richard P. Van Duyne, Laurence D. Marks, Segregation in bimetallic nanoparticles, Phys. Chem. Chem. Phys. V. **17**, 27940-27951(2015).

[32] Chunhua Cui, Lin Gan, Marc Heggen, Stefan Rudi, Peter Strasser, Compositional segregation in shaped Pt alloy nanoparticles and their structural behavior during electrocatalysis, Nat. Mate. V. **12**, 765–771(2013).

[33] Chen Chen, Yijin Kang, Ziyang Huo, Zhongwei Zhu, Wenyu Huang, Huolin L. Xin, Joshua D. Snyder, Dongguo Li, Jeffrey A. Herron, Manos Mavrikakis, Miaofang Chi, Karren L.More,Yadong Li, NenadM.Markovic, Gabor A. Somorjai, Peidong Yang, Vojislav R. Stamenkovic, Highly Crystalline Multimetallic Nanoframes with Three-Dimensional Electrocatalytic Surfaces, Science, V. **343**, 1339-1342(2014).

[34] Kuan-Wen Wang, Shu-Ru Chung, Chen-Wei Liu, Surface Segregation of PdxNi100-x Alloy Nanoparticles, J. Phys. Chem. C, V. **112**, 10242–10246(2008).

[35] R. H. Fowler and L. Nordheim, Electron Emission in Intense Electric Fields, Proceedings of the Royal Society of London. Series A, Containing Papers of a Mathematical and Physical Character, V. **119**, No. 781, 173-181 (1928).

[36] W. J. Huang, R. Sun, J. Tao, L. D. Menard, R. G. Nuzzo, J. M. Zuo,

Coordination-dependent surface atomic contraction in nanocrystals revealed by coherent diffraction, Nature Materials, V. **7**, 308-313(2008).

[37] A. C. Nunes, D. Lin, Effects of surface relaxation on powder diffraction patterns of very fine particles, J. Appl. Cryst. V. **28**, 274-278(1995).

[38] Kenji Ishikawa, Takatoshi Uemori, Surface relaxation in ferroelectric perovskite, Phys. Rev. B V. **60**, 11841-11845(1999).

[39] C. W. Mays, J. S. Vermaak, D. Kuhlmann-Wilsdorf, On surface stress and surface tension II. determination of the surface stress of gold, Surface Science, V. **12**, 134-140(1968).

[40] C. Solliard, M. Flueli, Surface stress and size effect on the lattice parameter in small particles of gold and platinum, Surface Science, V. **156**, 487-494(1985).

[41] Q. Jiang, L. H. Liang, D. S. Zhao, Lattice Contraction and Surface Stress of fcc Nanocrystals, J. Phys. Chem. B, V. **105**(27), 6275-6277(2001).

[42] Wilhelm G. Wolfer, Elastic properties of surfaces on nanoparticles, Acta Materialia, V. **59**, 7736 – 7743(2011).

[43] Yuanjie Huang, Electric features of dislocations and electric force between dislocations, Math. Mech. Sol. V. **26**(4), 616-628 (2021).

[44] Yuanjie Huang, Possible Source of The Earth's Geomagnetic Field, viXra: 1709.0024.

[45] Kenji Ishikawa, Takatoshi Uemori, Surface relaxation in ferroelectric perovskites, Phys. Rev. B V. **60**(17), 11 841-11845(1999).

[46] R. M. Wang, O. Dmitrieva,M. Farle, G. Dumpich,H. Q. Ye,H. Poppa,2 R. Kilaas, C. Kisielowski, Layer Resolved Structural Relaxation at the Surface of Magnetic FePt Icosahedral Nanoparticles, Phys. Rev. Lett., V. **100**, 017205(1-4) (2008).

[47] Giuseppe Grosso, Giuseppe Pastori Parravicini, Solid State Physics, Elsevier (Singapore) Pte Ltd. 1st edition, 2006, pp.397, pp. 427-429, pp.434, pp. 469-471.

[48] Debanjana Ghosh, Nitin Chattopadhyay, Gold and silver nanoparticle based Superquenching of fluorescence: A review, Journal of Luminescence, V. **160**, 223-232(2015).

[49] Bhogale, N. Patel, J. Mariam, P.M. Dongre, A. Miotello, D.C. Kothari, Comprehensive studies on the interaction of copper nanoparticleswith bovine serum albumin using various spectroscopies, Colloids and Surfaces B: Biointerfaces, V. **113** 276– 284(2014).

[50] Fleischmann, M.; Hendra, P.J.; McQuillan, A.J. Raman spectra of pyridine adsorbed at a silver electrode. Chem. Phys. Lett. V. **26**, 163–166(1974).

[51] Jeanmaire, D.L.; Van Duyne, R.P. Surface Raman spectroelectrochemistry. J. Electroanal. Chem. Interfacial Electrochem. V. **84**, 1–20(1977).

[52] Albrecht, M.G.; Creighton, J.A. Anomalously intense Raman spectra of pyridine at a silver electrode. J. Am. Chem. Soc. V. **99**, 5215–5217(1977).

[53] Song-Yuan Ding, En-Ming You, Zhong-Qun Tian, Martin Moskovits, Electromagnetic theories of surface-enhanced Raman spectroscopy, Chem. Soc. Rev. V. **46**, 4042-4076(2017).

[54] Roberto Pilot, Raffaella Signorini, Christian Durante, Laura Orian, Manjari

Bhamidipati, Laura Fabris, A Review on Surface-Enhanced Raman Scattering, Biosensors, V. **9**, 57(1-100)(2019).

[55] Judith Langer, Dorleta Jimenez de Aberasturi, Javier Aizpurua, Ramon A. Alvarez-Puebla, Baptiste Auguié, *et al*. Present and Future of Surface-Enhanced Raman Scattering, ACS Nano. V. **14**, 28−117(2020).

[56] Le Ru, E.C.; Etchegoin, P.G. Principles of Surface Enhanced Raman Spectroscopy; Elsevier: Amsterdam, The Netherlands, 2009.

[57] Paul L. Stiles, Jon A. Dieringer, Nilam C. Shah, Richard P. Van Duyne, Surface-Enhanced Raman Spectroscopy, Annu. Rev. Anal. Chem. V. **1**, 601-626(2008).

[58] A.G.Milekhin, L.L.Sveshnikova, T.A.Duda, N.A.Yeryukov, E.E.Rodyakina, A.K.Gutakovskii, S.A.Batsanov, A.V.Latyshev, D.R.T.Zahn, Surface-enhanced Raman spectroscopy of semiconductor nanostructures, Physica E, V. **75**, 210–222(2016).

[59] Niccolò Michieli, Roberto Pilot, Valentina Russo, Carlo Scian,Francesco Todescato, Raffaella Signorini, Stefano Agnoli,Tiziana Cesca,Renato Bozio, Giovanni Mattei, Oxidation effects on the SERS response of silver nanoprism arrays, RSC Adv., V. **7**, 369–378(2017).

[60] Xiaotian Wang, Wensheng Shi, Guangwei She, Lixuan Mu, Surface-Enhanced Raman Scattering (SERS) on transition metal and semiconductor nanostructures, Phys. Chem. Chem. Phys., V. **14**, 5891–5901(2012).

[61] Ying Gao, Nan Gao, Hongdong Li, Xiaoxi Yuan, Qiliang Wang, Shaoheng

Cheng, Junsong Liu, Semiconductor SERS of diamond, Nanoscale, V. **10**, 15788-15792(2018).

[62] Tamitake Itoh, Yuko S. Yamamoto, Reproduction of surface-enhanced resonant Raman scattering and fluorescence spectra of a strong coupling system composed of a single silver nanoparticle dimer and a few dye molecules, J. Chem. Phys. V. **149**, 244701(1-11) (2018).

[63] Ken-ichi Yoshida, Tamitake Itoh, Hiroharu Tamaru, Vasudevanpillai Biju, Mitsuru Ishikawa, Yukihiro Oza, Quantitative evaluation of electromagnetic enhancement in surface-enhanced resonance Raman scattering from plasmonic properties and morphologies of individual Ag nanostructures, Phys. Rev. B V. **81**, 115406(1-9) (2010).

[64] E. C. Le Ru, P. G. Etchegoin, Principles of Surface-Enhanced Raman Spectroscopy and related plasmonic effects, 1st edition, Elsevier B. V., Oxford, UK, 2009.

[65] Jianfeng Li, Yifan Huang, Yong Ding, Zhilin Yang, Songbo Li, Xiaoshun Zhou, Fengru Fan, Wei Zhang, Zhiyou Zhou, Deyin Wu, Bin Ren, Zhonglin Wang, Zhongqun Tian, Shell-isolated nanoparticle-enhanced Raman spectroscopy, Nature, V. **464**, 392-395(2010).

[66] Jian-Feng Li, Yue-Jiao Zhang, Song-Yuan Ding, Rajapandiyan Panneerselvam, Zhong-Qun Tian, Core−Shell Nanoparticle-Enhanced Raman Spectroscopy, Chem. Rev., V. **117**(7):5002-5069(2017).

[67] Felix Benz, Mikolaj K. Schmidt, Alexander Dreismann, Rohit Chikkaraddy, Yao

Zhang, Angela Demetriadou, Cloudy Carnegie, Hamid Ohadi, Bart de Nijs, Ruben Esteban, Javier Aizpurua, Jeremy J. Baumberg, Single-molecule optomechanics in "picocavities", Science V. **354** (6313), 726-729(2016).

[68] Hyun-Hang Shin, Gyu Jin Yeon, Han-Kyu Choi, Sang-Min Park, Kang Sup Lee, Zee Hwan Kim, Frequency-Domain Proof of the Existence of Atomic-Scale SERS Hot-Spots, Nano Lett. V. **18**, 262−271(2018).

[69] M. Moskovits, D. P. DiLella, K. J. Maynard, Surface Raman Spectroscopy of a Number of Cyclic and Molecular Reorientation Aromatic Molecules Adsorbed on Silver: Selection Rules, Langmuir, V. **4**(1), 61-76(1988).

[70] K. Kneipp, M. Moskovits, H. Kneipp (Eds.): Surface-Enhanced Raman Scattering-Physics and Applications, Topics Appl. Phys. V. **103**, 125-146 (2006).

[71] Q. J. Huang, X. Q. Li, J. L. Yao, B. Ren, W. B. Cai, J. S. Gao, B. W. Mao, Z. Q. Tian, Extending surface Raman spectroscopic studies to transition metals for practical applications III. Effects of surface roughening procedure on surface-enhanced Raman spectroscopy from nickel and platinum electrodes, Sur. Sci., 427–428, 162–166 (1999).

[72] W.B. Cai, B. Ren, X.Q. Li, C.X. She, F.M. Liu, X.W. Cai, Z.Q. Tian, Investigation of surface-enhanced Raman scattering from platinum electrodes using a confocal Raman microscope: dependence of surface roughening pretreatment, Surface Science, V. **406**, 9–22(1998).

[73] P. G. Cao, J. L. Yao, B. Ren, B. W. Mao, R. A. Gu, Z. Q. Tian, Surface-enhanced Raman scattering from bare Fe electrode surfaces, Chemical

Physics Letters, V. **316**, 1–5(2000).

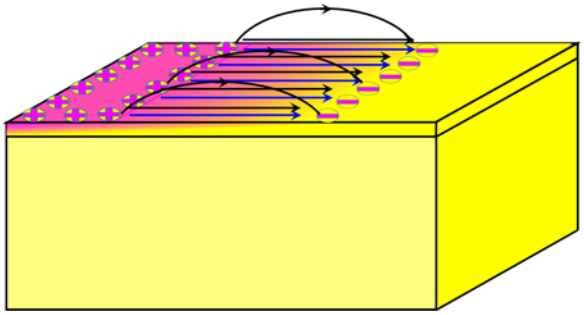

Figure 1 Schematic diagram of the tangential electrostatic field (TEF) at metal surfaces. Magenta regions denote the metal surface with higher Fermi surface energy (FSE), while yellow regions show the lower-FSE regions of the metal. Positive and negative signs represent positive and negative charges, respectively. Blue arrows stand for the TEF at the metal surfaces and the black ones denote the electrostatic field outside the metal surface.

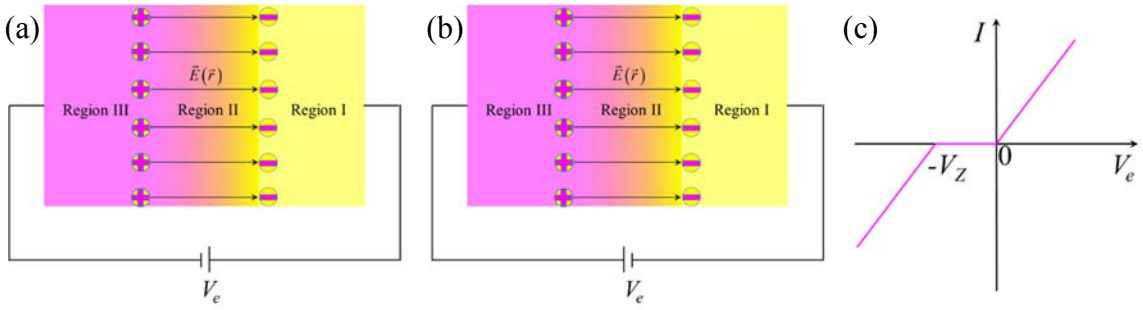

Figure 2. Electrical current-voltage (*I*-*V*) relation for the metal surface with a tangential electrostatic field (TEF). Region I (colored yellow) and region III (colored magenta) denote places with lower Fermi surface energy (FSE) and higher FSE, respectively, while region II shows the transition zone between region I and region III. (a) forward bias voltage; (b) backward bias voltage; (c) *I*-*V* characteristics.

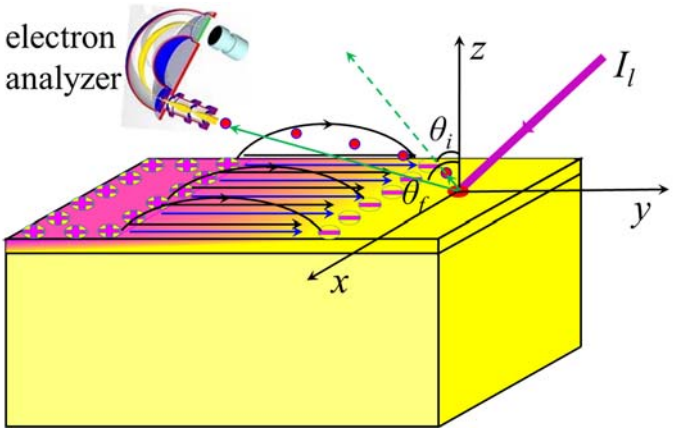

Figure 3 Sketch of photoemission spectroscopy (PES) affected by tangential electrostatic field at metal surface. When a light beam (colored purple) radiates at the metal surface, some photoelectrons (red dots) would be emitted and their motion would be influenced by the electrostatic field near the surface.

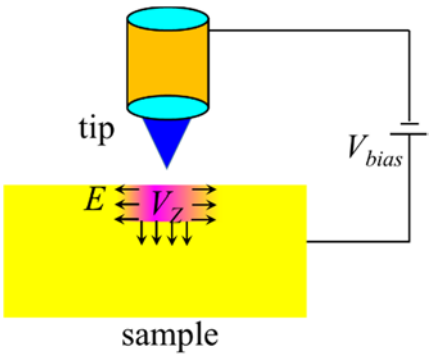

Figure 4. A bias voltage V_{bias} between tip of scanning tunneling microscope (STM) and metal surface with up-shifted Fermi surface energy (FSE) colored magenta. The up-shifted FSE may make this region possess a positive electric potential V_z and the surrounding electric field is shown by black arrows.

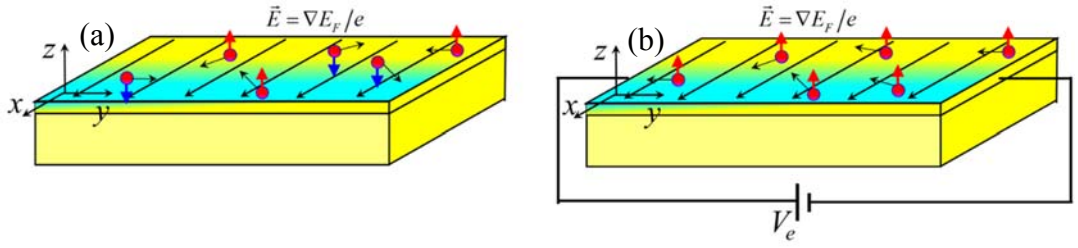

Figure 5. Momentum dependence (short black arrows) of polarized electron spins under a tangential electrostatic field at the metal surface. The tangential field is along x axis as indicated the long black arrows. The red circled present electrons. Red arrows and blue arrows denote the polarization direction of electron spins. (a) without external electrical voltage; (b) with an electrical voltage V_e.

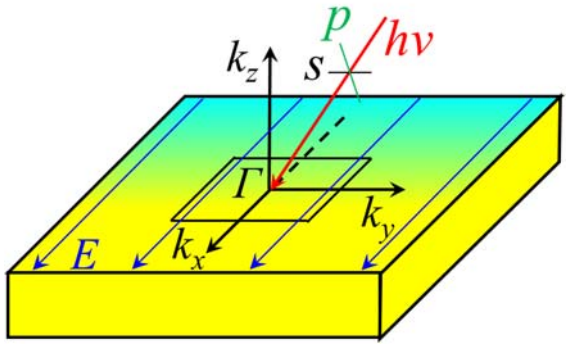

Figure 6 Schematic diagram of a beam of photons (denoted by red line) with s polarization (photon electric field perpendicular to the scattering plane k_x-k_z) or p polarization (photon electric field lying in the scattering plane k_x-k_z) radiating at a metal surface with tetragonal symmetry. The tangential electrostatic field indicated by blue arrows is along k_x direction.

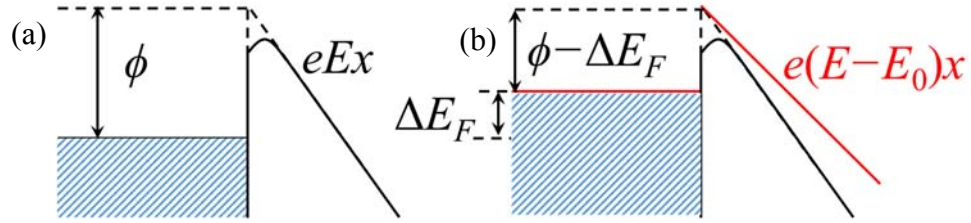

Figure 7. Sketch of field emission for a metal. (a) electron emission for the metal with a work function ϕ under an intense field E at metal surface; (b) electron emission for the region with a shifted Fermi surface energy (FSE) by the amount ΔE_F and the related electric field is changed to be E-E_0 where E_0 results from the shifted FSE.

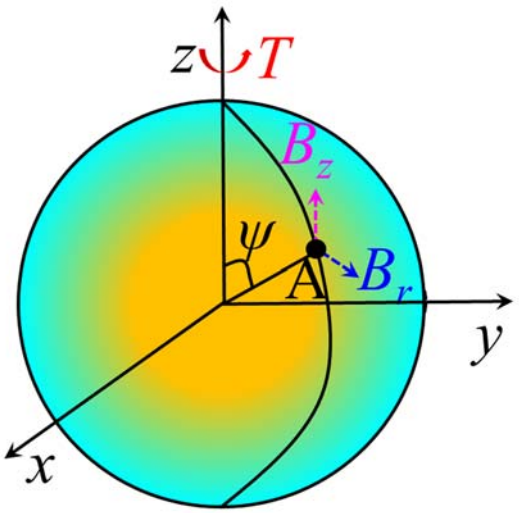

Figure 8. Schematic diagram of a magnetic dipole field yielded by fast rotation of a metal nanoparticle.

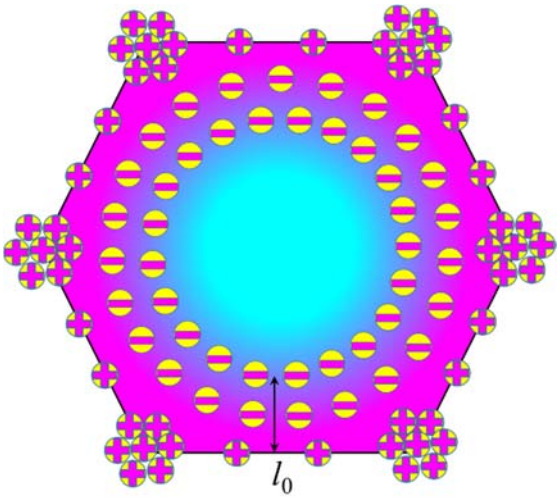

Figure 9. Sketch of cutaway drawing for a nanoparticle with charge separation. The strain (magenta zone and the strain relaxation length l_0) due to surface relaxation may exist along radius and cause the related remarkable charge separation. The net charges at surface may mainly distribute at the sharp edges and corners.

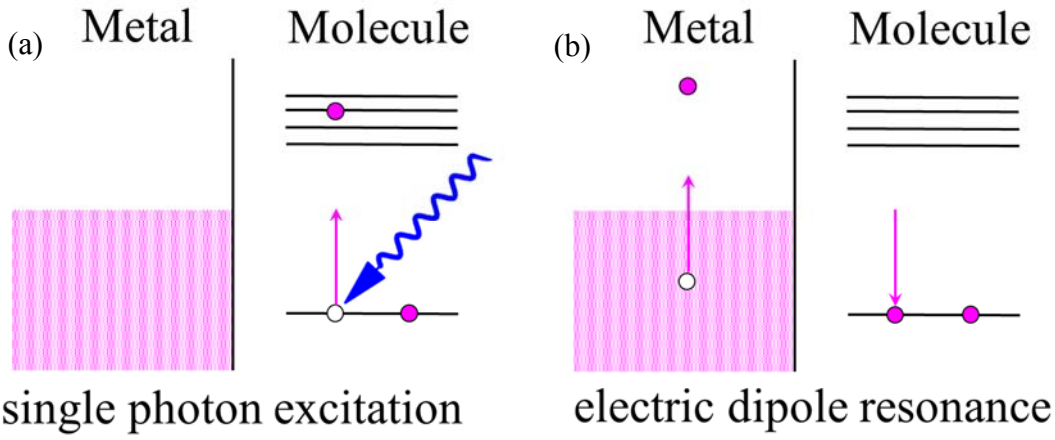

Figure 10. Schematic diagram of a possible mechanism for suppression of fluorescence owing to electric dipole resonance. The magenta circled represents electrons, the blue curved arrow stands for an incident photon and the magenta arrows show the electron hopping between different states (black horizontal lines). (a) single photon absorption process at the molecule; (b) electron energy transfer by means of electric dipole resonance between the molecule (right) and an adjacent metallic nanoparticle (left).

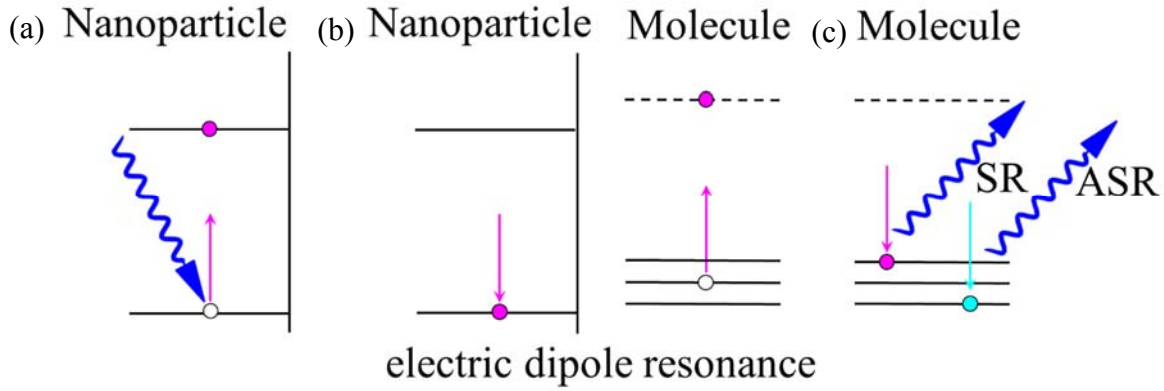

Figure 11. Schematic diagram of quantum processes for surface enhanced Raman scattering (SERS). (a) creation of an electron excitation by absorbed a photon (curved blue arrow); (b) the energy transfer in terms of electron double-dipole resonance (EDDR) between nanoparticle and adsorbed molecules; (c) emission of Stokes Raman (abbreviated SR) emission or emission of Anti- Stokes Raman (abbreviated ASR) photon.

Table 1. Binary continuous solid solutions according to the reference [30].

The groups in periodic table	Continuous solid solutions ($0 \leq x \leq 1$)			
Main group 1	Cs_xRb_{1-x}	K_xRb_{1-x}		
Main group 4	Ge_xSi_{1-x}			
Main group 5	Bi_xSb_{1-x}			
Main group 6	Se_xTe_{1-x}			
Subgroups 5, 6	Cr_xV_{1-x}	Mo_xTa_{1-x}	Mo_xV_{1-x}	Nb_xTa_{1-x}
Subgroups 5, 6	Mo_xW_{1-x}	Nb_xV_{1-x}	Nb_xW_{1-x}	Mo_xNb_{1-x}
Subgroups 5, 6	Ta_xW_{1-x}	V_xW_{1-x}		
Subgroups 7, 8	Os_xRu_{1-x}	Os_xRe_{1-x}	Re_xRu_{1-x}	
Subgroups 10,11	Ag_xPd_{1-x}	Ni_xPd_{1-x}	Ag_xAu_{1-x}	